Gradient lithiation to load controllable, high utilization lithium in graphitic carbon host for Li metal batteries

Lei Tao[1], Bingyuan Ma[1], Fenqiang Luo, Zhengrui Xu, Zhifeng Zheng, Haibo Huang, Peng Bai, Feng Lin

Dr. L. Tao, Z. Xu, Prof. F. Lin
Department of Chemistry
Virginia Tech, Blacksburg, Virginia 24061, USA
E-mail: fenglin@vt.edu

B. Ma, Prof. P. Bai
Department of Energy, Environment & Chemical Engineering
Washington University in St. Louis
St. Louis, MO 63130, USA

F. Luo, Prof. Z. Zheng
Fujian Engineering and Research Center of Clean and High-valued Technologies for Biomass, College of Energy
Xiamen University, Xiamen 361102, P.R. China

Prof. H. Huang
Department of Food Science and Technology
Virginia Tech, Blacksburg, Virginia 24061, USA

Keywords: Graphitic carbon paper, thermal infiltration, gradient lithiation, dendrite-free, Li metal batteries

Abstract: The multiphase interaction between Li metal and carbon materials provides great opportunities to design advanced composite anodes for Li metal batteries. Herein, we report the conversion of single-sheet graphitic carbon papers (CPs) to function-gradient Li/C composite anodes with controllable formations of LiC_6 and Li metal through controlling the thermal infiltration time. The uniform and dense lithiophilic LiC_6 is formed first and gradually covers the entire CP host, which promotes the subsequent homogeneous infiltration of metallic Li into the CP. The resulting composite anode has a unique gradient structure, with one example consisting of a lithiated LiC_6 coating of 5.8 mAh cm^{-2} and a thin Li bottom layer of 2.7 mAh cm^{-2}. Such a gradient composite structure allows for the selective utilization of Li metal and LiC_6 as the active component under different electrochemical conditions. This composite anode, with a much leaner Li loading than many reported Li/C composite anodes, has a stable porous framework and abundant lithiophilic sites, which enables uniform local electric field and stable Li metal deposition during cycling. Paired with high-capacity cathodes, the composite anode, with only a fraction of Li metal loading compared to Li foil, can provide better long-term cycling stability, and higher rate capability.

Introduction

Lithium-ion batteries have an attractive prospect for large-scale applications in electric vehicles and grid energy storage.[1,2] Although the development of batteries is in full swing, the increase in practical energy density appears to be far from meeting the market demand.[3,4] Lithium ion batteries have hit a bottleneck because of the limited theoretical capacity of graphite anode (~372 mAh g^{-1}). When developing new anode materials that meet the overall energy density requirements of future battery systems, researchers have revived lithium metal anode research because of its high theoretical capacity (~3860 mAh g^{-1}) and low electrochemical potential (-3.04 V vs. standard hydrogen electrodes).[5,6] However, some thorny issues have impeded its practical application, such as uncontrolled Li dendrites,[7,8] fragile solid electrolyte interphase (SEI),[9,10] and large volume changes during Li plating/stripping.[11,12]

Tremendous efforts have been devoted to combating these issues, such as designing new electrolyte components,[13,14] building stable SEIs,[15,16] constructing artificial SEIs,[17,18] engineering solid electrolytes,[19–21] as well as optimizing the metallic Li anode structure.[22,23] Among these approaches, constructing a structural Li electrode with 3D hosts has been considered as one of the most promising strategies for stabilizing Li metal batteries, changing the “hostless” Li to be “hosted” Li to mitigate the volume change for suppressing dendrites growth.[24] Such an approach is compatible with both liquid and solid electrolytes. Many different hosts have been developed, including metal framework,[25,26] porous carbon matrix,[27,28] as well as polymeric matrix[29] to fabricate 3D composite anodes through electrochemical deposition and thermal infiltration. We have previously reported a porous carbon membrane as a Li host to mitigate the volume change, inhibit dendritic growth and offer a long lifespan.[30,31] However, most Li hosts cannot be directly infiltrated by molten Li. Most of them require further surface modification or the introduction of lithiophilic atoms,[32–36] which usually involve tedious and sometimes aggressive reaction conditions (e.g., strong acid treatment). Furthermore, the modified hosts react rapidly and violently with molten Li; thus, the molten Li can uncontrollably occupies the entire pores of the host

in a short period, resulting in an extremely excessive Li metal loading.[37,38] These composite anodes have a dense inner structure similar to bulk Li foil, leaving no extra space to alleviate the volume change during Li plating/stripping, especially under high-capacity cycling conditions.[39] In addition, excessive Li metal loading far exceeds the practical demand, which leads to low battery energy density and low Li utilization.[40] Electrochemical Li deposition can be used to synthesize Li/C composite anode with controllable Li loading. However, side reactions during Li deposition can significantly undermine the yield of metallic Li[31,41] Therefore, there is a need to develop a novel Li composite anode with controllable Li loading for achieving high energy density Li metal batteries.

In this work, we propose a stable lithiated composite electrode achieved by directly contacting the highly graphitic carbon paper (CP) with molten Li. The CP is first shallowly lithiated to form a uniform, dense LiC_6 coating layer homogeneously throughout the CP host. Such a lithiophilic LiC_6 layer induces a strong capillary force that drives the molten Li to gradually infiltrate into the shallowly lithiated CP host, forming a gradient loading of metallic Li. To experimentally demonstrate the concept, we fabricate a lithiated composite electrode with 2.7 mAh cm^{-2} contributed by metallic Li and 5.8 mAh cm^{-2} contributed by lithiated LiC_6. The thin metallic Li layer is present only at the bottom (away from the separator) of the host without filling the inner space, which is favorable to accommodate the volume change during Li deposition. Meanwhile, the lithiophilic LiC_6 layer covers the entire host, promoting stable Li plating/stripping during battery cycling. As a result, the lithiated composite electrode offers good cycling stability and rate capability in both symmetric cells and high-capacity full cells.

Results and discussion

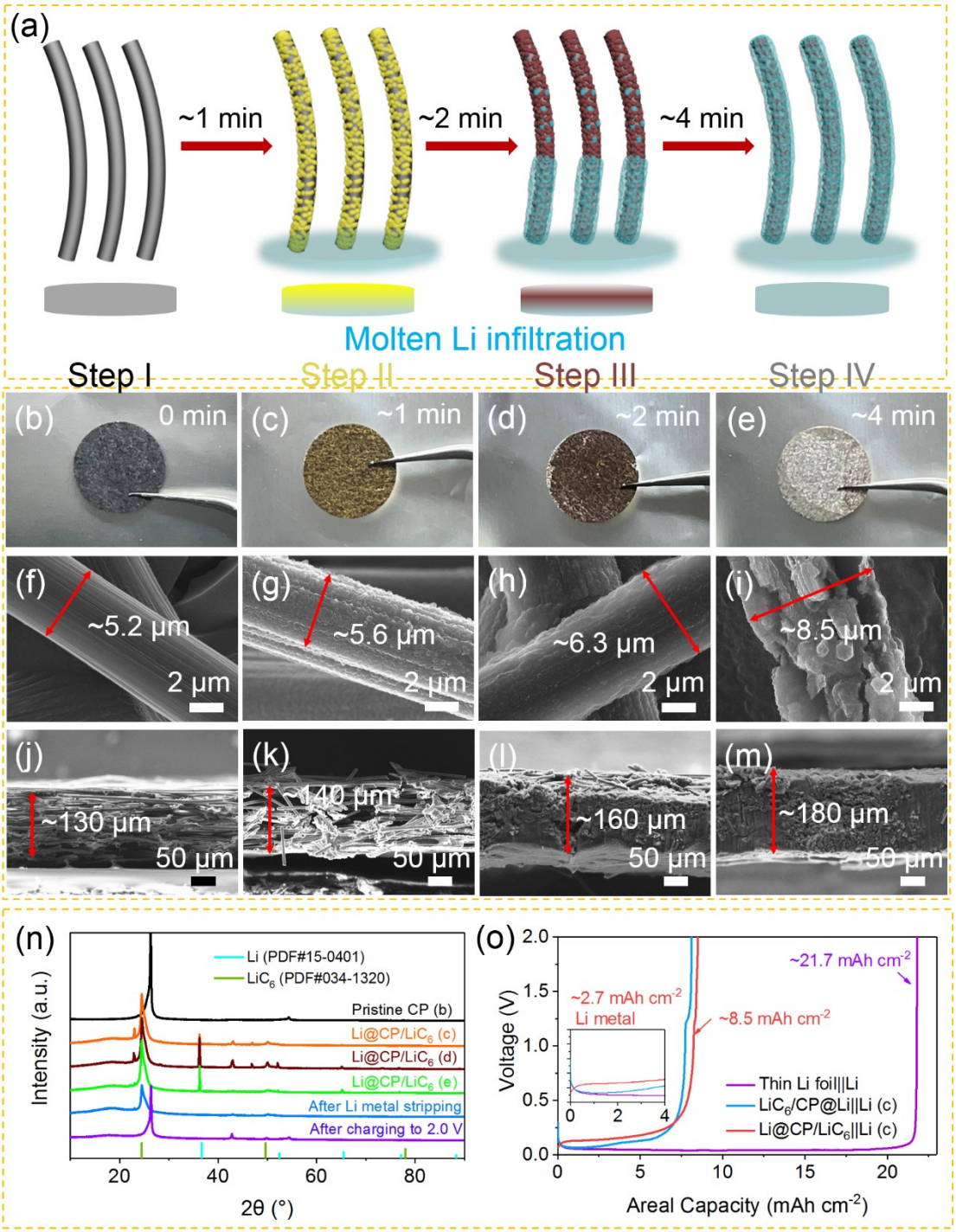

Figure 1. (a) Schematic of the fabrication process of the Li@CP/LiC_6 electrode (Gray cylinder: Carbon fiber; Golden-yellow sphere: LiC_6; Brown sphere: part of Li metal covering the LiC_6; Cyan: Molten Li). (b-e) Digital photos of the color evolution of the Li@CP/LiC_6 electrode when molten Li gradually infiltrates into CP. Corresponding SEM images of the Li@CP/LiC_6 electrode at (f-i) high-magnification top view, and (j-

m) cross-section view. (n) The XRD pattern of the Li@CP/LiC_6 electrode at different steps from (b) to (e). (o) The stripping profiles of the thin Li foil||Li, LiC_6/CP@Li||Li (LiC_6 towards the bottom side, away from separator) and Li@CP/LiC_6||Li(LiC_6 towards the top side, next to separator) half cells after charging to 2.0 V at a current density of 1.0 mA cm^{-2}.

The fabrication process of the Li@CP/LiC_6 electrode is shown in **Figure 1a** and Video S1. The pristine CP without any modifications is placed on top of the molten Li at ~400 °C. In the course of just a few minutes, the color of CP changed from black (Step I) to golden-yellow (Step II), then brown (Step III), and finally silver (Step IV), indicating that the molten Li can intercalate and infiltrate the CP host (Figure 1a-1e) uniformly. Note that the brown color (Fig. 1d) is due to the incomplete coverage of the golden-yellow LiC_6, not to be confused with the red color of the partially lithiated Stage II graphite.[42] It is also noteworthy that other 3D hosts are difficult to be directly infiltrated by molten Li due to their weak lithiophilicity, requiring further modifications, such as doping lithiophilic element (N-, O-)[28,31] or forming Li alloys (Zn, Sn).[37,43] Herein, the commercial carbon paper (CP) is chosen as the host to accommodate Li metal due to its highly graphitic structure (Figure S1, supporting information), excellent resistivity (5.6 mΩ·cm) as well as abundant porous structure (Figure 1f, >78% porosity). According to the Gibbs free energy change of the lithiation reaction ($Li + 6C \rightarrow LiC_6$, -10.59 kJ mol^{-1}) [44] between graphitic carbon and metallic Li, Li atoms spontaneously intercalate into the graphitic carbon to form lithiated LiC_6 compounds once CP is in contact with Li metal. Meanwhile, the high temperature promotes the reaction to proceed rapidly, producing uniform and dense lithiophilic LiC_6 layer on the fiber surface. Furthermore, the capillary force of the porous CP structure drives the gradual infiltration of molten Li into the 3D framework of CP, which forms the Li@CP/LiC_6 electrode with a controllable Li loading depending on the reaction time (Figure 1c-1e).[45,46] Figures 1f-1m illustrate the morphological evolution of CP during the lithiation and Li infiltration process. The pristine CP is composed of interwoven fibers with a smooth surface (Figure 1f) and has a thickness of ~130 μm (Figure 1j). After

lithiation, small particles homogeneously and densely cover the fiber surface (Figure 1g, Step II), accompanied by a thin Li metal layer of ~10 μm on the bottom side of CP (Figure S2, supporting information). Upon further infiltration, the molten Li climbs to the fibers that are already covered by the lithiophilic LiC_6 layer, and gradually spreads into the porous structure of CP (Figure 1d, 1h, Step III), increasing the apparent thickness to ~160 μm (Figure 1l). The molten Li continues to spread until it completely fills the 3D framework of CP (Figure 1e, 1i, Step IV), and the thickness further increases to ~180 μm (Figure 1m). The XRD pattern also shows the evolution of CP diffraction peak during the lithiation and Li infiltration process. The pristine CP exhibits an evident graphitic carbon diffraction peak at 26.3°, and then migrates to 24.5° after lithiation denoting the formation of LiC_6 compounds (Figure 1n).[47] The new diffraction peaks at about 36.2°, 52.0°, and 65.0° correspond to the (110), (200), and (211) planes of the metallic Li (*PDF#15-0401*), suggesting a high Li crystallinity of the composite anode.[30] Notably, the peak intensity of LiC_6 does not further increase, illustrating that the CP has been completely lithiated to form LiC_6 when the color of CP changes to golden-yellow. Therefore, the subsequent color evolution corresponds to the infiltration of molten Li, accompanied by a gradual increase in the peak intensity of metallic Li (Figure 1n). According to the SEM images of Figure 1l and 1m, it can be clearly seen that the pristine CP porous structure has been filled with metallic Li (Step IV), which is not conducive to the effective utilization of Li metal. For example, when such a composite anode is cycled in a full cell, the effect is the same as that of the Li foil because it has no extra space to accommodate the deposited Li metal, which causes the deposited Li metal to accumulate on the surface of the composite anode. During the repeated cycling, the accumulation layer may cause the formation/growth of Li dendrites and dead Li, resulting in lower Li metal utilization. In contrast, after lithiation and partial infiltration of metallic Li (Figure 1c, Step II), the Li@CP/LiC_6 electrode still maintains a large amount of lithiophilic sites, rich porosity, fast mass transport channels, and low resistance (Figure S3, supporting information) to guide Li^+ uniform deposition and accommodate the volume changes, which can effectively promote dendrite-free

plating/stripping behavior, and fully improve the utilization of Li metal. Therefore, we choose Step II Li@CP/LiC_6 electrode for further experiments.

The Li content of the Li@CP/LiC_6 electrode is further quantified by electrochemical measurements. The stripping profile shows that the complete Li capacity of the Li@CP/LiC_6 electrode is about 8.5 mAh cm^{-2} after charging to 2.0 V at a current density of 1.0 mA cm^{-2}, where the capacities contributed by metallic Li and lithiated LiC_6 are 2.7 and 5.8 mAh cm^{-2}, respectively (Figure 1o). This is further confirmed by the corresponding SEM and XRD results. After stripping 3.0 mAh cm^{-2} Li from the Li@CP/LiC_6 electrode, the lithiophilic LiC_6 layer still covers the fiber surface, and the electrode color maintains golden-yellow, while the underlying Li metal is almost fully stripped (Figure S4, supporting information). The small amount of Li residue may be due to the high stripping current dentisty and the side reaction of Li-electrolyte, which makes the bottom Li metal difficult to completely strip in a short time. However, the amount of Li should be minimal, because the corresponding XRD pattern does not show the diffraction peak of metallic Li (Figure 1n, blue line). After charging to 2.0 V, the lithiated LiC_6 completely disappears, and the color of CP host becomes close to the pristine color (Figure S5, supporting information). Additionally, the Li@CP/LiC_6 electrode still maintains an intact porous structure, confirming the high structural stability of the CP framework. Meanwhile, the LiC_6 peak shifts to 26.3°, attributable to the graphitic carbon peak (Figure 1n, purple line). These results demonstrate that the bottom Li layer is stripped prior to the lithiated LiC_6, promoting the utilization of Li metal. The carbon host has a porous structure, which means that stripping the bottom Li layer has no ion transport limitation. Furthermore, several studies have also shown that the higher delithiation potential of lithiated LiC_6 ensures the complete stripping of the Li metal before the delithiation of LiC_6.[48] Once the metallic Li is completely consumed, the LiC_6 will participate in the delithiation reaction to replenish the Li source and sustain the cell cycling.

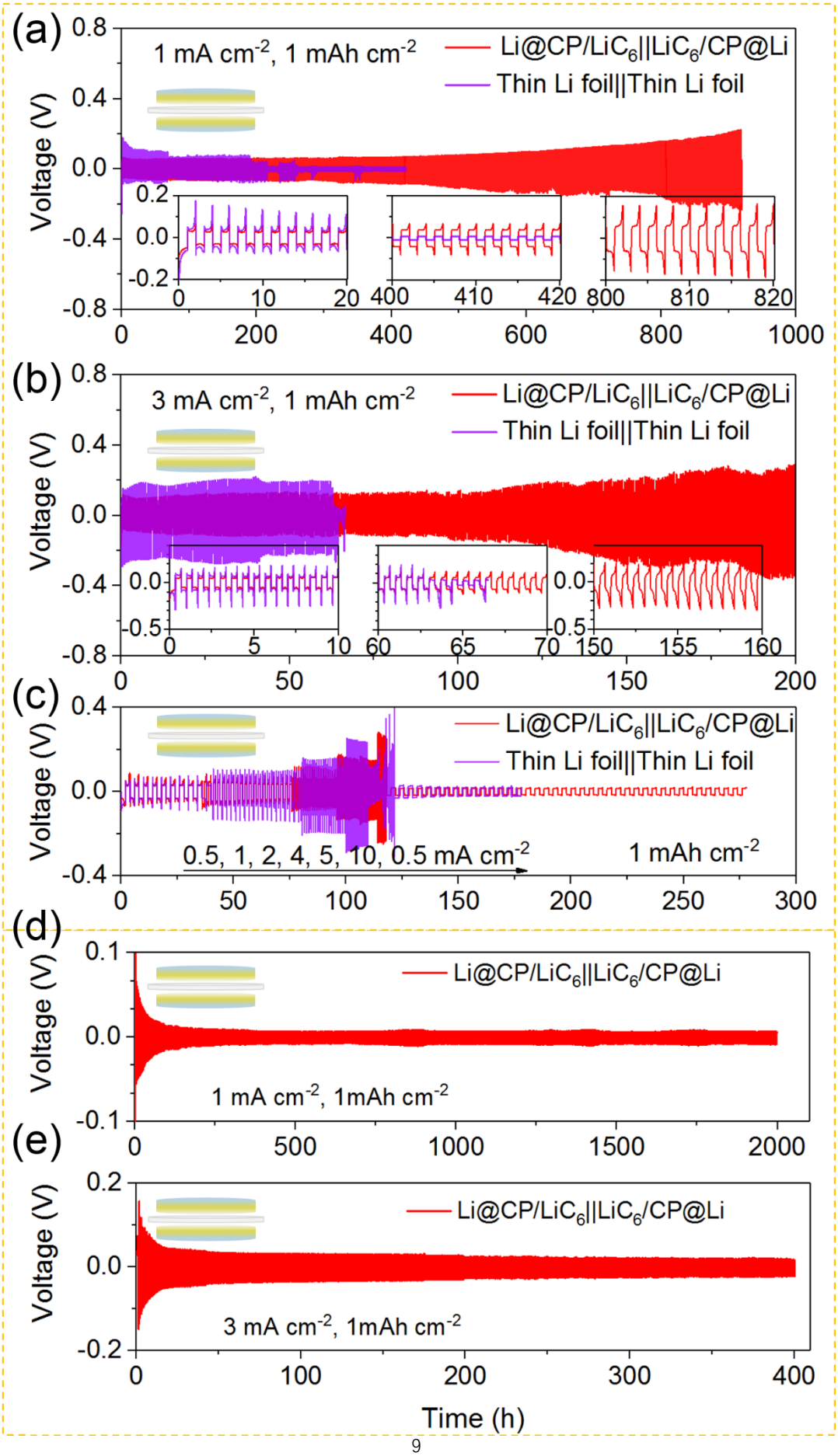
(a)
1 mA cm-2, 1 mAh cm-2
Li@CP/LiC6||LiC6/CP@Li
Thin Li foil||Thin Li foil
Voltage (V)
(b)
3 mA cm-2, 1 mAh cm-2
Li@CP/LiC6||LiC6/CP@Li
Thin Li foil||Thin Li foil
Voltage (V)
(c)
Li@CP/LiC6||LiC6/CP@Li
Thin Li foil||Thin Li foil
0.5, 1, 2, 4, 5, 10, 0.5 mA cm-2
1 mAh cm-2
Voltage (V)
(d)
Li@CP/LiC6||LiC6/CP@Li
1 mA cm-2, 1mAh cm-2
Voltage (V)
(e)
Li@CP/LiC6||LiC6/CP@Li
3 mA cm-2, 1mAh cm-2
Voltage (V)
Time (h)

Figure 2. Voltage profiles of the symmetric cells based on the Li@CP/LiC_6 and thin Li foil electrodes measured at (a) 1 mA cm^{-2}, (b) 3 mA cm^{-2}, and (c) rate capability (0.5 to 10 mA cm^{-2}) for 1 mAh cm^{-2} Li plating and stripping in carbonate-based electrolyte (1M $LiPF_6$ in EC/EMC with 2 wt.% VC) at 22 °C. (e, f) The Li@CP/LiC_6 symmetric cells were measured in the same configurations in an ether-based electrolyte (1M LiTFSI in DOL/DME with 1wt.% $LiNO_3$) at 22 °C. The schemes inserted in each panel represent the configuration of the symmetric cells, which all have the LiC_6 layers against the separator.

Symmetric cells are tested at different current densities to further evaluate the long-term cycling stability of the Li@CP/LiC_6 electrode. The thin Li foil is assembled in the same configurations for comparison. We first evaluate the symmetric cell performance in the conventional carbonate-based electrolyte (1M $LiPF_6$ in EC/EMC with 2wt.%VC). **Figure 2a** shows voltage profile of both symmetric cells at a current density of 1 mA cm^{-2}, with a Li plating/stripping capacity of 1 mAh cm^{-2}. The Li@CP/LiC_6 symmetric cell exhibits good cycling stability with a much smaller voltage hysteresis for over 600 h (300 cycles). In contrast, the thin Li foil symmetric cell undergoes a stable cycling with a large voltage hysteresis in the first 200 h (100 cycles), but overpotential fluctuations occur in the following cycles, indicating the severe Li dendritic growth. By increasing the current density to 3 mA cm^{-2} (Figure 2b), the Li@CP/LiC_6 symmetric cell still demonstrates better cycling stability for more than 120 h (180 cycles), while the control cell quickly experiences an internal short circuit in less than 70 h (105 cycles). While its voltage hysteresis slightly increases during long-term cycling, the Li@CP/LiC_6 symmetric cell does not fail (at 1 mA cm^{-2} after 600 h or at 3 mA cm^{-2} after 120 h, respectively). When cycled in the carbonate-based electrolyte, the limited metallic Li loading in the Li@CP/LiC_6 electrode is gradually consumed, and delithiation of LiC_6 is required to compensate, resulting in a slight increase in interfacial impedance. The rate capability of both symmetric cells is also comparable (Figure 2c). Importantly, the voltage hysteresis of the Li@CP/LiC_6 symmetric cell increases with increasing current density and keeps steady at 10 mA cm^{-}

^{2}. As the current density restores to 0.5 mA cm^{-2}, the overpotential recovers, followed by stable cycling for more than 160 h, which indicates that the Li@CP/LiC_6 electrode has good rate capability to endure high current density and satisfactory reversibility. In contrast, the thin Li foil symmetric cell exhibits large voltage polarization at low current densities (< 4 mA cm^{-2}) and then quickly shorts at 5 mA cm^{-2} due to Li dendrite formation.

Next, we also evaluate the symmetric cell performance in an ether-based electrolyte (1 M LiTFSI in DOL/DME with 1 wt.% $LiNO_3$), which is known to have better compatibility with Li metal (Figure S6, supporting information).[49] The Li@CP/LiC_6 symmetric cell exhibits much lower voltage hysteresis and maintain ultra-long-term cycling performance for 2000 h (1000 cycles) without significant voltage fluctuations or overpotential elevation (Figure 2d). Even if the current density is increased to 3.0 mA cm^{-2}, the Li@CP/LiC_6 symmetric cell can still cycle stably for 400 h (600 cycles) with a consistently low voltage hysteresis (Figure 2e). The excellent cycling stability of the Li@CP/LiC_6 electrode can be potentially attributed to the uniformly distributed lithiophilic LiC_6 throughout the entire 3D framework, which enables stable Li plating and stripping, and minimizes the consumption of active Li metal.

We further measure the electrochemical impedance spectroscopy (EIS) of symmetric cells cycled in the carbonate-based electrolyte. Figure S7 shows the impedance evolution at different cycles measured at 1 mA cm^{-2} with 1 mAh cm^{-2} Li plating/stripping. The Li@CP/LiC_6||LiC_6@CP/Li symmetric cell shows much lower interfacial impedance than that of the thin Li foil symmetric cell after the same cycle numbers, indicating that the former has a stable Li plating/stripping process. Moreover, the impedance of both symmetric cells gradually increases after 100 cycles. This result is consistent with the voltage hysteresis of previous symmetric cell cycling (Figure 2a), that is, the cells cycle in commercial carbonate electrolyte is more likely to react with Li metal to form an unstable SEI layer, resulting in the formation/growth of Li dendrites and increasing resistance. However, compared to the Li foil symmetric cell with severe

Li dendritic growth, the impedance of cycled Li@CP/LiC_6 electrode only increases slightly, further indicating a more stable electrolyte-electrode interphase for uniform Li plating/ stripping has been achieved in the Li@CP/LiC_6 composite electrode.

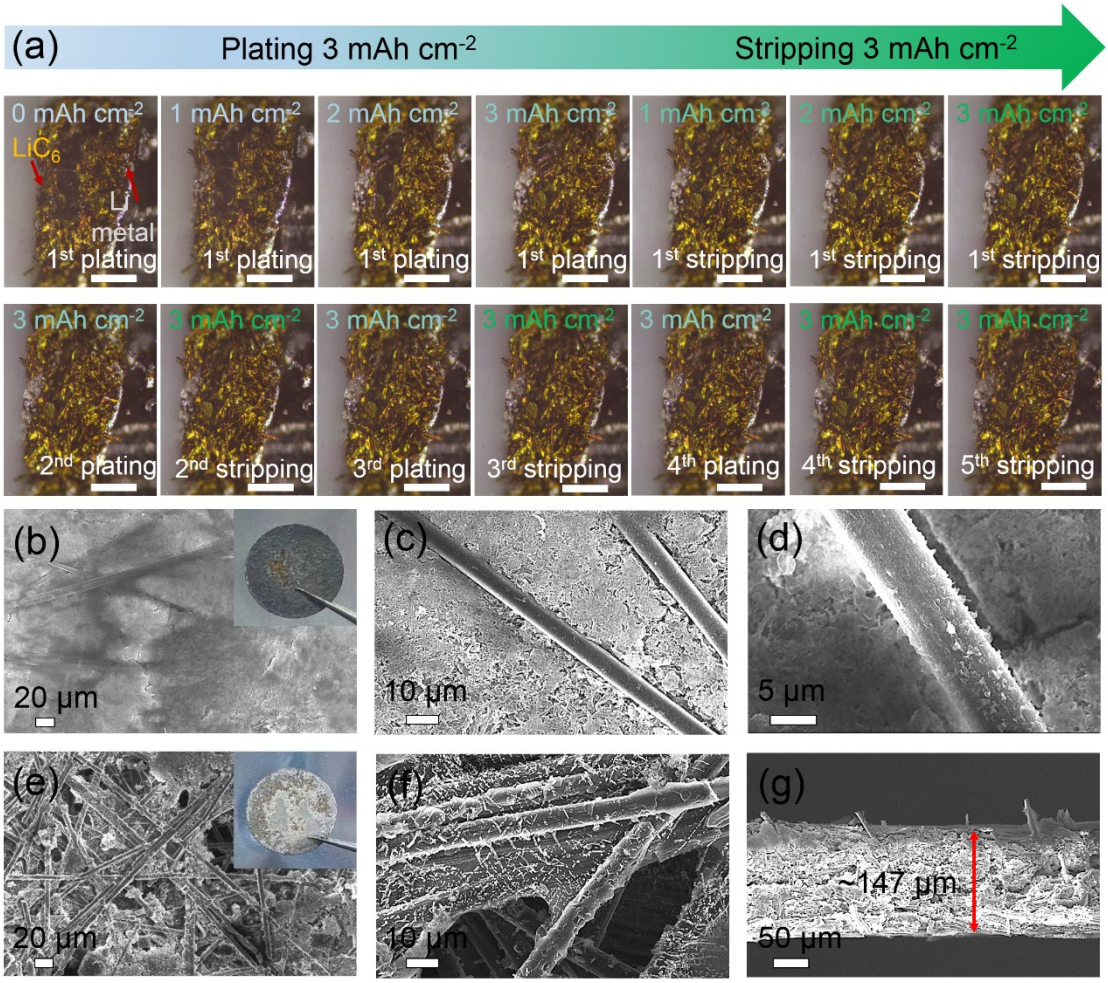

Figure 3. (a) *Operando* optical microscopic images of the Li@CP/LiC_6 electrode-electrolyte interphase (left side: LiC_6 facing separator, right side: Li metal away from separator) measured at 0.5 mA cm^{-2} with 3 mAh cm^{-2} Li plating/stripping process for 5 cycles (scale bar: 50 μm). SEM images of the (b, c, d) top facing separator, (e, f) bottom away from the separator, and (g) cross-sectional view of the Li@CP/LiC_6 electrode cycling in the Li@CP/LiC_6||LiC_6/CP@Li symmetric cell after 100 cycles. Insets: Optical photos of the (b) top and (e) bottom view of the Li@CP/LiC_6 electrode after 100 cycles. The electrochemical measurement is performed in carbonate electrolyte (1M $LiPF_6$ in EC/EMC with 2 wt.% VC) at 22 °C.

To visualize the stability of the Li@CP/LiC_6 symmetric cell during cycling, we fabricated miniature transparent cells in glass capillaries [50,51] and performed an *operando* optical microscopic experiment to monitor the Li plating/stripping process. **Figure 3a** and Video S2 demonstrate the time-lapse images of the Li@CP/LiC_6 electrode in the cross-sectional view measured at 0.5 mA cm^{-2} with 3 mAh cm^{-2} Li plating/stripping. The pristine Li@CP/LiC_6 electrode is covered with uniform lithiophilic LiC_6 and has a thin Li metal bottom layer. After 1 mAh cm^{-2} Li plating, the Li@CP/LiC_6 electrode has no visible volume change. Most of the Li metal is stored in the pores of the electrode while only a small fraction of Li metal is deposited on the LiC_6 side due to the strong lithiophilic properties. Upon further plating to 2.0 mAh cm^{-2}, the Li metal is still evenly deposited within the 3D porous structure and even reaching the bottom, which effectively avoids the formation and growth of Li dendrites. Even after plating to 3.0 mAh cm^{-2}, the Li@CP/LiC_6 electrode still maintains the pristine thickness and the plated Li metal can be stored uniformly. As expected, no Li dendritic formation/growth is observed during the Li plating process. During the subsequent stripping process, the plated Li metal gradually disappears without impairing the bulk structure (Figure 3a). With the deep stripping to 3.0 mAh cm^{-2}, it can be clearly observed that the bottom layer Li metal (right side) participates in the stripping (more details can be observed in Video S2). Also, no "dead" Li can be observed from the LiC_6 side (electrode/electrolyte interface) during the entire stripping process. Video S2 shows several cycles of the subsequent Li plating and stripping process under the same conditions. The Li@CP/LiC_6 electrode can fully withstand the deep Li plating and stripping without any structural damage or thickness increase. Benefiting from the unique structure of the Li@CP/LiC_6 electrode, most of the Li metal is plated and stripped in the 3D space of the electrode in the whole process, and there is no obvious "dead" Li layer accumulated on the electrode's surface. In contrast, the Li foil suffers from severe Li whisker/cluster growth (Video S3, and Figure S8, supporting information),[52,53] in which porous Li structrues were unevenly accumulated on the surface of Li foil and gradually aggravated as the Li deposition increases. The surface

plated Li shrinks during the Li stripping but does not disappear even after 3 mAh cm^{-2} of stripping, resulting in a "dead" Li layer covering the Li foil surface. After several cycles, "dead" Li almost completely covers the Li foil (Video S3, supporting information). Since the Li foil is covered by a thick accumulated SEI layer and "dead" Li, which blocks Li-ion transport and leads to increase of resistance and quick cell failure (Figure 2 and Figure S7, supporting information).

We also compare the SEM images of both electrodes cycled in the symmetric cell after 100 cycles at 1 mA cm^{-2} with 1 mAh cm^{-2} Li plating/stripping. The cycled Li@CP/LiC_6 electrode displays a relatively flat surface without Li dendrite/whisker formation (Figure 3b, 3c), and the lithiophilic LiC_6 still covers the individual fibers to enhance the strong binding between the CP host and Li-ions (Figure 3d)[44]. On the bottom face of the electrode, the bottom layer Li metal is gradually stripped during cycling (Figure 3e, 3f), thereby avoiding the accumulation of "dead" Li layers on the active Li metal to hinder the Li ion transport. The thickness of the cycled Li@CP/LiC_6 electrode does not increase, and there is no crack formation (Figure 3g), which is beneficial to provide a stable environment for Li plating and stripping. On the contrary, the cycled Li foil experiences an obvious thickening process with a layer of dead Li accumulates on the surface of Li metal (Figure S9 and Figure S10d, supporting information). In these regions, highly porous Li structures that are apparent disconnected "dead" Li are observed (Figure S10a-c, supporting information), which is the reason for the rapid failure of the Li-foil symmetric cell.

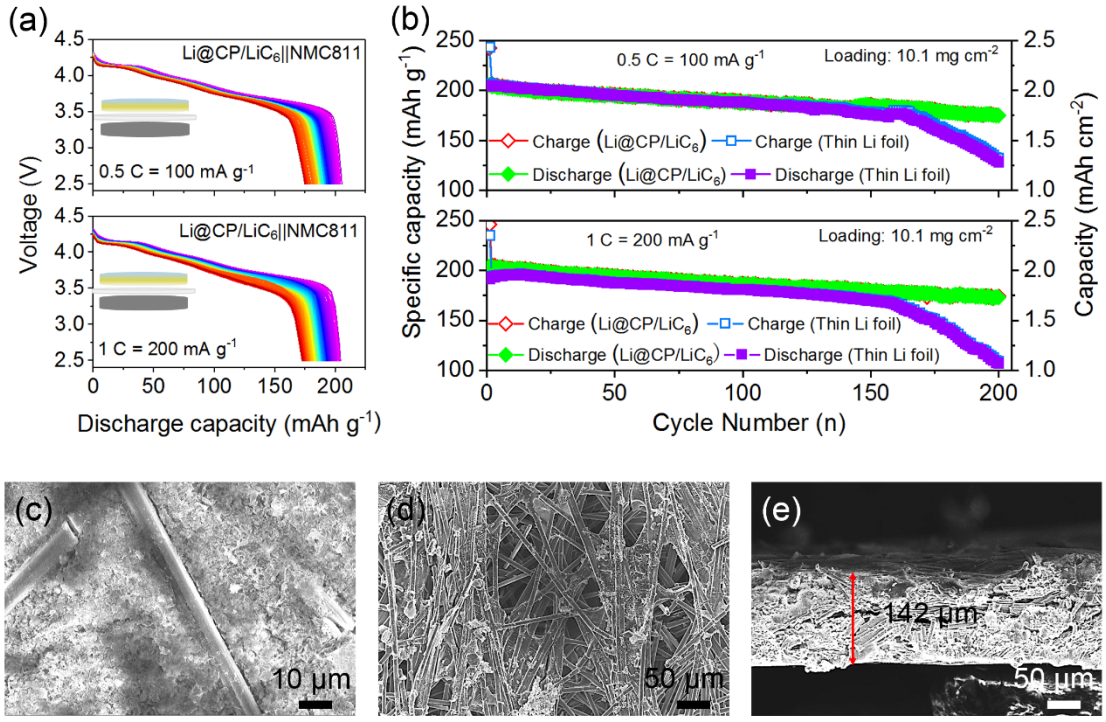

Figure 4. (a) Voltage profiles of Li@CP/LiC_6||NMC811 full cell cycled at 0.5 C and 1 C. (b) Corresponding long-term cycling performance of Li@CP/LiC_6||NMC811 and thin Li foil||NMC811 full cells at 0.5 C and 1 C, respectively. SEM images of the (c) top, (d) bottom, (e) cross-sectional view of the Li@CP/LiC_6 electrode after 160 cycles at 1 C. The electrochemical measurement is performed in carbonate electrolyte (1M $LiPF_6$ in EC/EMC with 2 wt.% VC) at 22 °C.

To further elucidate the potential use of the Li@CP/LiC_6 anode in full cells, we test two types of full cells in a coin cell configuration using a high capacity $LiNi_{0.8}Mn_{0.1}Co_{0.1}O_2$ (NMC811) cathode (~2.0 mAh cm^{-2}) and a high stability $LiFePO_4$ (LFP) cathode (~1.0 mAh cm^{-2}), respectively. For comparison, a Li foil with extremely excessive capacity is also paired with these cathodes. **Figure 4** and Figure S11 show the electrochemical performance of the NMC811 full cells, using Li@CP/LiC_6 anode (capacity: ~2.7 mAh cm^{-2} metallic Li, Figure 1o) and thin Li foil (capacity: ~21.7 mAh cm^{-2}, Figure 1o), respectively. Both full cells deliver a similar initial discharge capacity of ~204 mAh g^{-1}, with an areal capacity of ~2.0 mAh cm^{-2} at 0.5 C (Figure 4a, 4b, and Figure S11a, supporting information). Cycling a high-capacity cathode while maintaining good stability have strict requirements on the anode because the relatively

high Li% utilization of the anode in each cycle usually leads to consumption of Li metal,[40] especially for anodes with lean Li loading. Nevertheless, the Li@CP/LiC_6||NMC811 full cell exhibits much better cycling stability with a reversible capacity of ~175 mAh g^{-1} at 0.5 C after 200 cycles, which is ~86% capacity retention. In contrast, the thin Li||NMC811 full cell has poor cycling performance and experiences a rapid capacity decay after 165 cycles. When the current density increases to 1 C, the Li@CP/LiC_6||NMC811 full cell can still achieve 200 cycles and maintains ~86% capacity retention of its initial capacity of ~202 mAh g^{-1} (Figure 4a). In comparison, the thin Li||NMC811 full cell can only provide a lower initial discharge capacity of ~193 mAh g^{-1} and experience a significant capacity fading after 160 cycles (Figure 4b and Figure S11b, supporting information).

The metallic Li of the Li@CP/LiC_6 anode is only one-eighth of thin Li foil, while its cycling stability is more than 1.2 times that of the latter, indicating that the former has higher Li utilization and fewer side reactions with the electrolyte when cycled against a high-capacity cathode. We also highlight that the non-metallic Li in LiC_6 could have also helped stabilize the Li@CP/LiC_6 anode in the full cell cycling. We further investigate the anodes using SEM. The Li@CP/LiC_6 anode after 160 cycles against NMC811 shows a comparably flat surface with no major "dead" Li, and retains a similar thickness to its original state (Figure 4c-4e). On the contrary, the thin Li foil after 160 cycles against NMC811 exhibits a rough and loose structure with a thick, cracked "dead" Li layer above the active Li metal (Figure S12, supporting information). Moreover, we disassemble the cycled Li foil||NMC811 full cell (after 160 cycles) and replace the aged Li foil with a new piece. The renewed Li foil||NMC811 full cell once again shows stable cycling performance without significant capacity degradation (Figure S13, supporting information). Furthermore, we polish the cycled Li foil to remove the dead Li layer for reuse. The polished Li foil||NMC811 full cell can not only restore the capacity but also be cycled 40 times stably (Figure S14, supporting information), which corroborates that the capacity fading is mainly caused by the Li foil anode. In addition, the internal resistance of Li@CP/LiC_6||NMC811 full cell is much lower than that of the thin Li

foil||NMC811 full cell after the same cycle numbers (Figure S15, supporting information), suggesting better Li^+ transport kinetics and a stable interphase environment in the former. All of the above results demonstrate that the Li@CP/LiC_6 anode can provide homogeneous Li plating and stripping with a high Li% utilization with minimal side reactions, allowing for stable full-cell cycling performance.

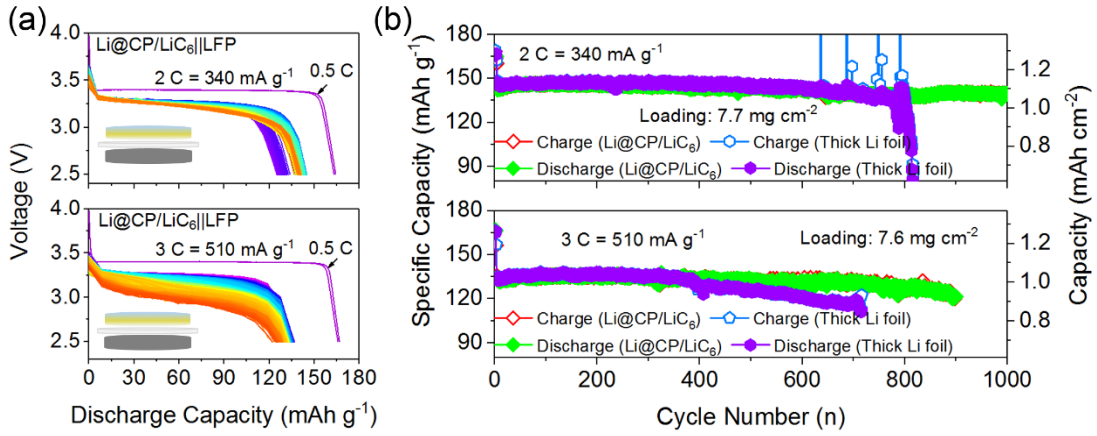

Figure 5. (a) Voltage profiles of Li@CP/LiC_6||LFP full cell cycled at 2 C and 3 C. (b) Corresponding long-term cycling performance of Li@CP/LiC_6||LFP and thick Li foil||LFP full cells at 2 C and 3 C, respectively. The electrochemical measurement is performed in carbonate electrolyte (1M $LiPF_6$ in EC/EMC with 2wt.% VC) at 22 °C. Before cycling at a high C rate, all cells are first cycled at 0.5 C for 2 cycles of activation, allowing the electrolyte to completely wet the porous electrode.

To show that the Li@CP/LiC_6 anode can also achieve good stability at high C rates, we choose high stability LFP cathode to assemble Li@CP/LiC_6||LFP full cells. Since the thin Li foil only sustains 160 cycles in the NMC811 full cells at low C rates, thus we try to use a thick Li foil (~400 μm, ~80 mAh cm^{-2}) instead of thin Li foil as the counterpart to ensure sufficient Li amount at high C rates. Both full cells are tested at 2 C and 3 C (1 C = 170 mAh g^{-1}). As shown in **Figure 5** and Figure S16, the Li@CP/LiC_6||LFP full cell exhibits long-term cycling stability for achieving 1000 cycles at 2 C with a reversible capacity of 136 mAh g^{-1}, corresponding to a capacity retention of 94%, whereas the thick Li foil||LFP full cell can only remain stable for less than 800 cycles before transitioning to much faster degradation. A similar result is observed at 3 C. The Li@CP/LiC_6||LFP full cell delivers a high reversible capacity of

121 mAh g^{-1} with a capacity retention of 90% after 900 cycles. In contrast, the thick Li foil||LFP full cell experiences rapid capacity fading after 700 cycles.

Although we significantly increase the Li loading by using a thick Li foil in the LFP full cell to improve long-term cycling stability, serious side reactions still occur in each cycle, resulting in a large amount of dead Li residues accumulating on Li metal, thus accelerating Li consumption and hindering Li-ion transport, eventually leading to rapid capacity decay. In stark contrast, our Li@CP/LiC_6 anode with a significantly lower Li loading can deliver superior cycling performance, which is attributed to the homogeneous Li plating/stripping behavior and stable host environment resulted from the lithiophilic LiC_6 in the porous CP host.

Conclusion

There is a strong incentive to improve Li% utilization and cycling stability of Li metal anode for practical Li metal batteries. In this work, we have designed a novel Li@CP/LiC_6 composite electrode by employing a commercial graphitic CP host to accommodate Li metal through thermal infiltration. Due to the negative Gibbs free energy change during the CP-Li reaction, a uniform, dense LiC_6 layer is spontaneously generated and gradually covers the carbon fibers. Upon further reaction, the molten Li is driven to infiltrate into the lithiated CP host with the assistance of capillary force, where the metallic Li loading can be controlled by changing the reaction time. Unlike the reported Li composite electrodes with excessive Li loading and dense inner structure, the Li@CP/LiC_6 composite electrode is composed of a much leaner 2.7 mAh cm^{-2} metallic Li loading at the bottom of the CP and an additional 5.8 mAh cm^{-2} Li coating layer in the form of LiC_6. Such a low metallic Li loading allows us to investigate the cycling stability of a lean Li anode in commercial carbonate electrolytes. Furthermore, the composite electrode still maintains abundant lithiophilic sites, high porosity, and high electrical conductivity, which can effectively mitigate Li dendritic growth and volume changes. Compared to Li foil, the Li@CP/LiC_6 composite electrode, with a much lower Li loading, exhibits not only much better cycling stability, higher

rate capability, and lower voltage hysteresis in symmetric cells, but also achieved higher capacity retention and longer lifespan in full cells paired with high-capacity NMC811 and LFP cathodes. This work provides an alternative strategy for designing a highly efficient and stable Li composite anode for high-energy-density Li metal batteries.

Reference

[1] Y. Liang, H. Dong, D. Aurbach, Y. Yao, *Nat. Energy* **2020**, *5*, 646.

[2] J. Xie, Y. C. Lu, *Nat. Commun.* **2020**, *11*, 2499.

[3] P. R. Shearing, L. R. Johnson, *Joule* **2020**, *4*, 1359.

[4] S. Chen, F. Dai, M. Cai, *ACS Energy Lett.* **2020**, *5*, 3140.

[5] J. Liu, Z. Bao, Y. Cui, E. J. Dufek, J. B. Goodenough, P. Khalifah, Q. Li, B. Y. Liaw, P. Liu, A. Manthiram, Y. S. Meng, V. R. Subramanian, M. F. Toney, V. V. Viswanathan, M. S. Whittingham, J. Xiao, W. Xu, J. Yang, X. Q. Yang, J. G. Zhang, *Nat. Energy* **2019**, *4*, 180.

[6] J. Y. Hwang, S. J. Park, C. S. Yoon, Y. K. Sun, *Energy Environ. Sci.* **2019**, *12*, 2174.

[7] A. Jana, S. I. Woo, K. S. N. Vikrant, R. E. Garcí, *Energy Environ. Sci.* **2019**, *12*, 3595.

[8] Y. Zhu, J. Xie, A. Pei, B. Liu, Y. Wu, D. Lin, J. Li, H. Wang, H. Chen, J. Xu, A. Yang, C. L. Wu, H. Wang, W. Chen, Y. Cui, *Nat. Commun.* **2019**, *10*. 2067.

[9] X. Cao, X. Ren, L. Zou, M. H. Engelhard, W. Huang, H. Wang, B. E. Matthews, H. Lee, C. Niu, B. W. Arey, Y. Cui, C. Wang, J. Xiao, J. Liu, W. Xu, J. G. Zhang, *Nat. Energy* **2019**, *4*, 796.

[10] J. Alvarado, M. A. Schroeder, T. P. Pollard, X. Wang, J. Z. Lee, M. Zhang, T. Wynn, M. Ding, O. Borodin, Y. S. Meng, K. Xu, *Energy Environ. Sci.* **2019**, *12*, 780.

[11] C. Fang, X. Wang, Y. S. Meng, *Trends Chem.* **2019**, *1*, 152.

[12] J. Lopez, A. Pei, J. Y. Oh, G. J. N. Wang, Y. Cui, Z. Bao, *J. Am. Chem. Soc.* **2018**, *140*, 11735.

[13] F. Li, J. He, J. Liu, M. Wu, Y. Hou, H. Wang, S. Qi, Q. Liu, J. Hu, J. Ma, *Angew. Chem. Int. Ed.* **2021**, *60*, 6600.

[14] Q. Wang, Z. Yao, C. Zhao, T. Verhallen, D. P. Tabor, M. Liu, F. Ooms, F. Kang, A. Aspuru-Guzik, Y. S. Hu, M. Wagemaker, B. Li, *Nat. Commun.* **2020**, *11*, 4188.

[15] D. Luo, L. Zheng, Z. Zhang, M. Li, Z. Chen, R. Cui, Y. Shen, G. Li, R. Feng, S. Zhang, G. Jiang, L. Chen, A. Yu, X. Wang, *Nat. Commun.* **2021**, *12*, 186.

[16] D. Cheng, T. A. Wynn, X. Wang, S. Wang, M. Zhang, R. Shimizu, S. Bai, H. Nguyen, C. Fang, M. cheol Kim, W. Li, B. Lu, S. J. Kim, Y. S. Meng, *Joule* **2020**, *4*, 2484.

[17] R. Xu, X.-B. Cheng, C. Yan, X.-Q. Zhang, Y. Xiao, C.-Z. Zhao, J.-Q. Huang, Q. Zhang, *Matter* **2019**, *1*, 317.

[18] M. L. Meyerson, P. E. Papa, A. Heller, C. B. Mullins, *ACS Nano* **2021**, *15*, 29.

[19] M. Balaish, J. C. Gonzalez-Rosillo, K. J. Kim, Y. Zhu, Z. D. Hood, J. L. M. Rupp, *Nature Energy* **2021**, *6*, 227.

[20] K. B. Hatzell, X. C. Chen, C. L. Cobb, N. P. Dasgupta, M. B. Dixit, L. E. Marbella, M. T. McDowell, P. P. Mukherjee, A. Verma, V. Viswanathan, A. S. Westover, W. G. Zeier, *ACS Energy Lett.* **2020**, *5*, 922.

[21] Q. Zhao, S. Stalin, C. Z. Zhao, L. A. Archer, *Nat. Rev. Mater.* **2020**, *5*, 229.

[22] P. Shi, X. Q. Zhang, X. Shen, R. Zhang, H. Liu, Q. Zhang, *Adv. Mater. Technol.* **2020**, *5*, 1900806.

[23] Z. Cao, B. Li, S. Yang, *Adv. Mater.* **2019**, *31*, 1901310.

[24] S. Park, H. J. Jin, Y. S. Yun, *Adv. Mater.* **2020**, *32*, 2002193.

[25] X. Y. Yue, X. L. Li, J. Bao, Q. Q. Qiu, T. Liu, D. Chen, S. S. Yuan, X. J. Wu, J. Lu, Y. N. Zhou, *Adv. Energy Mater.* **2019**, *9*, 1901491.

[26] X. Y. Yue, W. W. Wang, Q. C. Wang, J. K. Meng, X. X. Wang, Y. Song, Z. W. Fu, X. J. Wu, Y. N. Zhou, *Energy Storage Mater.* **2019**, *21*, 180.

[27] H. Chen, A. Pei, J. Wan, D. Lin, R. Vilá, H. Wang, D. Mackanic, H. G. Steinrück, W. Huang, Y. Li, A. Yang, J. Xie, Y. Wu, H. Wang, Y. Cui, *Joule* **2020**, *4*, 938.

[28] G. Huang, J. Han, F. Zhang, Z. Wang, H. Kashani, K. Watanabe, M. Chen, *Adv. Mater.* **2019**, *31*, 1805334.

[29] Y. Liu, D. Lin, Z. Liang, J. Zhao, K. Yan, Y. Cui, *Nat. Commun.* **2016**, *7*, 10992.

[30] L. Tao, A. Hu, Z. Yang, Z. Xu, C. E. Wall, A. R. Esker, Z. Zheng, F. Lin, *Adv. Funct. Mater.* **2020**, *30*, 2000585.

[31] L. Tao, Z. Xu, C. Kuai, X. Zheng, C. E. Wall, C. Jiang, A. R. Esker, Z. Zheng, F. Lin, *Energy Storage Mater.* **2020**, *24*, 129.

[32] Y. Liu, S. Xiong, J. Wang, X. Jiao, S. Li, C. Zhang, Z. Song, J. Song, *Energy Storage Mater.* **2019**, *19*, 24.

[33] K. H. Chen, A. J. Sanchez, E. Kazyak, A. L. Davis, N. P. Dasgupta, *Adv. Energy Mater.* **2019**, *9*, 1802534.

[34] Q. Yang, M. Cui, J. Hu, F. Chu, Y. Zheng, J. Liu, C. Li, *ACS Nano* **2020**, *14*, 1866.

[35] X. Chen, X.-R. Chen, T.-Z. Hou, B.-Q. Li, X.-B. Cheng, R. Zhang, Q. Zhang, *Sci. Adv.* **2019**, *5*, eaau7728.

[36] T. Zhou, J. Shen, Z. Wang, J. Liu, R. Hu, L. Ouyang, Y. Feng, H. Liu, Y. Yu, M. Zhu, *Adv. Funct. Mater.* **2020**, *30*, 1909159.

[37] Y. Zhang, C. Wang, G. Pastel, Y. Kuang, H. Xie, Y. Li, B. Liu, W. Luo, C. Chen, L. Hu, *Adv. Energy Mater.* **2018**, *8*, 1800635.

[38] B. Yu, T. Tao, S. Mateti, S. Lu, Y. Chen, *Adv. Funct. Mater.* **2018**, *28*, 1803023.

[39] S. Jiao, J. Zheng, Q. Li, X. Li, M. H. Engelhard, R. Cao, J. G. Zhang, W. Xu, *Joule* **2018**, *2*, 110.

[40] P. Albertus, S. Babinec, S. Litzelman, A. Newman, *Nat. Energy* **2018**, *3*, 16.

[41] D. J. Kautz, L. Tao, L. Mu, D. Nordlund, X. Feng, Z. Zheng, F. Lin, *J. Mater. Chem. A* **2018**, *6*, 16003.

[42] S. Agrawal, P. Bai, *Adv. Energy Mater.* **2021**, *11*, 2003344.

[43] W. Deng, W. Zhu, X. Zhou, F. Zhao, Z. Liu, *Energy Storage Mater.* **2019**, *23*, 693.

[44] P. Shi, T. Li, R. Zhang, X. Shen, X. B. Cheng, R. Xu, J. Q. Huang, X. R. Chen, H. Liu, Q. Zhang, *Adv. Mater.* **2019**, *31*, 1807131.

[45] Z. Y. Wang, Z. X. Lu, W. Guo, Q. Luo, Y. H. Yin, X. Bin Liu, Y. S. Li, B. Y.

Xia, Z. P. Wu, *Adv. Mater.* **2021**, *33*, 2006702.

[46] S. Huang, L. Chen, T. Wang, J. Hu, Q. Zhang, H. Zhang, C. Nan, L. Z. Fan, *Nano Letters* **2021**, *21*, 791.

[47] Y. Sun, G. Zheng, Z. W. Seh, N. Liu, S. Wang, J. Sun, H. R. Lee, Y. Cui, *Chem* **2016**, *1*, 287.

[48] Y. Liu, X. Qin, F. Liu, B. Huang, S. Zhang, F. Kang, B. Li, *ACS Nano* **2020**, *14*, 1837.

[49] X. B. Cheng, C. Yan, X. Chen, C. Guan, J. Q. Huang, H. J. Peng, R. Zhang, S. T. Yang, Q. Zhang, *Chem* **2017**, *2*, 258.

[50] Youngju Lee, Bingyuan Ma, Peng Bai, *Energy Environ. Sci.* **2020**, *13*, 3504.

[51] B. Ma, Y. Lee, P. Bai, *Adv. Sci.* **2021**, *8*, 2005006.

[52] Peng Bai, Ju Li, F. R. Brushett, M. Z. Bazant, *Energy Environ. Sci.* **2016**, *9*, 3221.

[53] P. Bai, J. Guo, M. Wang, A. Kushima, L. Su, J. Li, F. R. Brushett, M. Z. Bazant, *Joule* **2018**, *2*, 2434.

Supporting Information

Supporting Information is available from the Wiley Online Library or from the author.

Author Contribution

F. Lin conceived and led the project. L.T. performed materials synthesis, electrochemical measurements, and characterization. F. Luo and Z.X. helped with electrochemical measurements and SEM. B.M. and P.B. performed operando optical microscopic measurements. Z.Z. and H.H. participated in scientific discussion. L.T. and F. Lin analyzed all data and wrote the manuscript with assistance from all the coauthors. L.T. and B. M. contributed equally to this work.

Acknowledgments

This work was supported by the USDA AFRI Foundational and Applied Program (grant number 2020-67021-31139) and the Institute for Critical Technology and Applied Science at Virginia Tech. H. H. acknowledges the support from the Virginia Agriculture Experiment Station and the Hatch Program of the National Institute of Food and Agriculture (NIFA), USDA.

Conflict of Interest

The authors declare no conflict of interest.

Received: ((will be filled in by the editorial staff))
Revised: ((will be filled in by the editorial staff))
Published online: ((will be filled in by the editorial staff))